Constitutive modelling and mechanical characterization of aluminium-based metal matrix composites produced by spark plasma sintering

Gabriella Bolzon [a,*], Enzo J. Chiarullo [a], Pedro Egizabal [b], Claude Estournes [c]

[a] *Dipartimento di Ingegneria Strutturale, Politecnico di Milano, Italy*
[b] *Fundación Inasmet-Tecnalia, San Sebastián, Spain*
[c] *CNRS, Institut Carnot CIRIMAT, F-31062 Toulouse, France*

A B S T R A C T

Spark plasma sintering has been applied to the production of aluminium-based functionally graded material systems to be used in abrasive and high temperature conditions. The overall mechanical properties of these metal matrix composites were determined during the optimization phases of the production process by a fast and reliable identification procedure based on instrumented indentation, which can be easily performed on small specimens. The experimental information gathered from conical (Rockwell) indentation was used as input data for the calibration of the material parameters entering the elastic–plastic Drucker–Prager constitutive model. Eventually, the so identified material parameters were used to predict the result of pyramidal (Vickers) indentation, in order to validate the model selection and the output of the identification procedure. The good matching between modelling and experimental results for the different test configurations confirmed the soundness of the considered approach, especially evidenced on the light of the strong influence on the overall mechanical characteristics of the material microstructure and defectiveness resulting from the production process, which prevent the use of classical homogenization rules to evaluate the macroscopic material properties.

Keywords:
Metal matrix composites
Spark plasma sintering (SPS)
Material characterization
Instrumented indentation
Drucker–Prager constitutive model
Parameter identification

1. Introduction

Functionally graded materials can be conceived as layered structures with progressively varying composition. The material system under investigation is constituted by a pure aluminium (Al) intermediate core coated by different zirconia (ZrO_2) and titanium diboride (TiB_2) reinforced layers, designed in order to present good wear characteristics in the side with high TiB_2 content and significant mechanical resistance at high temperatures in the opposite side, rich in ZrO_2.

The material has been produced by spark plasma sintering (SPS); see Omori (2000), Ichikawa (2001), and Hulbert et al. (2009). The target characteristics were obtained by a preliminary optimization of the production process of each Al/TiB_2 and Al/ZrO_2 layer.

The overall mechanical properties of the single composite layers under investigation have been experimentally determined during the optimization phase of the sintering process. The reduced size of the specimens obtained during the preliminary production steps prevented material characterization by standard tests. A parameter calibration methodology has been considered then, based on instrumented indentation and inverse analysis, according to a spreading approach that combines measured and modelled specimen response (Giannakopoulos and Suresh, 1997; Bhushan, 1999; Venkatesh et al., 2000; Dao et al. 2001; Capehart and Cheng, 2003; Bolzon et al., 2004, 2008; Bocciarelli and Bolzon, 2007; Bocciarelli et al., 2008).

Experimental information gathered from conical indentation brought input data to the material characterization procedure, which returned the parameters entering the

* Corresponding author. Tel.: +39 02 2399 4319; fax: +39 02 2399 4220.
E-mail address: Gabriella.bolzon@polimi.it (G. Bolzon).

doi:10.1016/j.mechmat.2010.03.001

selected constitutive model at the macro-scale. Eventually, the model selection and the identified parameter set were validated by the prediction of the results of Vickers indentation, further performed in the same material specimens.

Beyond the elastic limit, it is often assumed that the overall response of metal-ceramic composites is governed by the metal behaviour. Pressure-insensitive constitutive laws, like the classical Hencky–Huber–Mises (HHM) model, are therefore mostly considered at the macro-scale; see, e.g. the recent work by Giannakopoulos (2002), Gu et al. (2003), and Bhattacharyya et al. (2007).

In the alternative proposal by Bocciarelli et al. (2008), volume fractions govern the transition from HHM model toward the more general Drucker–Prager (DP) constitutive law, more suitable to describe the mechanical behaviour of ceramics.

One purpose of the present research was to verify the reliability of the above hypotheses for the aluminium-based composites under investigation.

The effect of microstructure details on the overall mechanical performances has been further investigated. In the technical literature, in fact, constitutive parameters at the macroscopic scale are mostly assumed to depend on the local material properties of the primary composite phases, neglecting the role of voids and defects as they are confined to small volumes. Homogenization rules have been then developed to relate the constitutive parameters (mainly, elastic constants) of composites to the volume content of their components only, e.g. by the classical Reuss and Voigt mixture laws or by popular modification of these formulae, like the one developed for metal alloys by Tamura et al. (1973) and thereafter applied to different heterogeneous material systems; see e.g. Nakamura et al. (2000) and Jin et al. (2003). Investigations carried out, e.g., by Bruck and Rabin (1999) suggested instead that micro-structural details may play a major role as local damages like micro-cracking or particle debonding develops. Therefore, the possible correspondence of the identified mechanical properties with their prediction by classical homogenization rules has been further discussed.

2. Production of the composite samples

The composite material samples considered in the present investigation have been produced by Inasmet-Tecnalia (San Sebastian, Spain) in collaboration with CNRS at the SPS National Platform (PNF2-CNRS) located at the Université Paul Sabatier in Toulouse (France), where a Dr Sinter SPS2080 equipment is available. The SPS process, used in the case of conductive samples, let a pulsed direct current pass through a graphite die containing a powder mixture as well as the powder itself. Heat is thus internally generated and the reactions that lead to the formation of the eventual compounds take place in few minutes. Fully compacted metals and ceramics can be obtained by carefully selecting the different starting materials. For the present application, raw Al and ZrO_2 powders of about 45 μm grain size were considered, while TiB_2 grain size was in the range 5–45 μm.

Fig. 1 shows a scanning electron microscope (SEM) image of an Al/TiB_2 layer containing around 50% weight of TiB_2 particles. The material has been produced in about 5 min at a processing temperature of 530 °C, under 50 MPa pressure (2.5 kN force applied on a 8 mm inner diameter graphite die). In the picture, lighter particles are TiB_2 while Al appears dark grey. Some individual boron particles (size range 15–40 μm) and some porosity is left (black inclusions), the estimated volume fraction of voids being less than 3%. The large size range of the TiB_2 particles is related both to the initial size distribution of the TiB_2 powder and to the possible grinding of particulates during processing.

Fig. 2 shows a SEM image of the Al/ZrO_2 layer with 40% weight ceramic content, produced at 580 °C under 100 MPa pressure. Zirconia particulates appear as light grey while aluminium is the dark phase. The microstructure is quite homogeneous and the average porosity level, obtained by measuring the actual composite density by Archimede's method and comparing the result with its theoretical value for the given component content ratio, is lower than 1%.

The resulting random microstructure permits to assume isotropic material response.

The characteristics of each metal matrix composite layer influence significantly the overall mechanical properties of the target compound, but the small material volumes obtained during the optimization of the production process do not allow direct measurements of constitutive parameters of interest like elastic modulus, yield limit, hardening coefficient, internal friction angle of the designed composites.

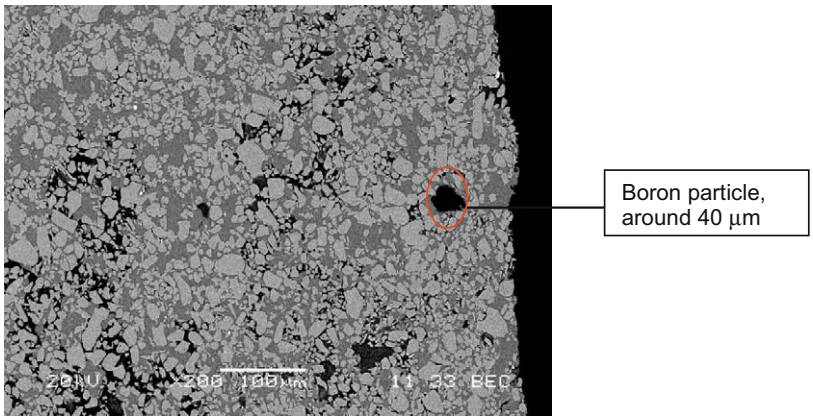

Fig. 1. SEM image of Al/TiB_2 composite produced by SPS at 530 °C under 50 MPa pressure.

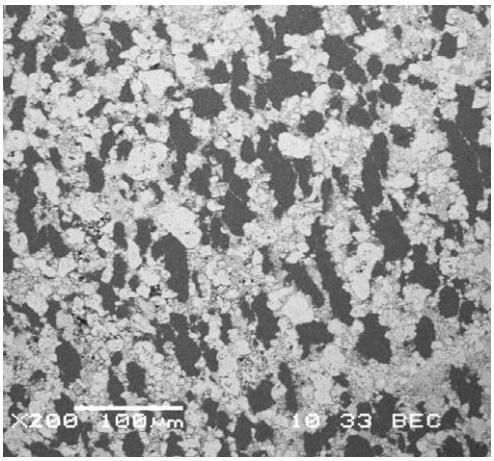

Fig. 2. SEM image of Al/ZrO_2 composite produced by SPS at 580 °C under 100 MPa pressure.

Instrumented indentation was then exploited to the present identification purposes. This is a fast and flexible experiment to be performed either directly on structural components or in small material specimens, more and more commonly employed in industrial environments to return reliable estimates of several material parameters, although the quantitative interpretation of this test results is not always immediate. The informative content of the experimental data collected during indentation can be profitably exploited to material characterization purposes by combined experimental-numerical procedures. The inverse analysis methodology developed by Bolzon et al. (2004) and Bocciarelli et al. (2008) has been implemented in the present case to recover material parameters contained in the DP formulation and to verify the capability of this constitutive model to represent the real behaviour of the available Al/TiB_2 and Al/ZrO_2 composite specimens. Results have been verified making use of independent experimental information collected from different indentation tests.

3. Selected constitutive model

The mechanical behaviour beyond the elastic range of metal matrix composites is often hypothesised to be essentially governed by the spreading of plasticity into the metal phase, and the material response is therefore described by classical Hencky–Huber–Mises (HHM) plasticity, see e.g. Nakamura et al. (2000) and Jin et al. (2003).

Bocciarelli et al. (2008) proposed to replace HHM model by the more general Drucker–Prager (DP) formulation, which includes HHM as a special case but better describes the mechanical behaviour of ceramics and, therefore, of composites with high ceramic content. HHM constitutive law, in fact, implicitly assumes the material response to be the same in tension and in compression and to be insensitive to hydrostatic stresses. These hypotheses are well verified by metals but do not apply to most ceramics.

DP yield criterion with linear isotropic hardening reads:

$$f = \sqrt{\frac{1}{2}\sigma'_{ij}\sigma'_{ij}} + \alpha I_1 - k - h\lambda \leq 0 \tag{1}$$

where σ'_{ij} denote the components of the deviatoric stress tensor; I_1 represents the first stress invariant, i.e. the trace of the tensor collecting the stress components σ_{ij}; λ (>0) is the cumulative multiplier of the plastic deformations, which develop as $f = 0$ and $\dot{f} \geq 0$ (the superimposed dot denotes a rate quantity); α, k and h are material parameters in this constitutive model.

The internal friction angle α and the initial cohesion k depend on the initial tensile and compressive yield limits, σ_{t0} and σ_{c0}, respectively, as follows:

$$\alpha = \sqrt{3}\frac{\sigma_{c0} - \sigma_{t0}}{(\sigma_{c0} + \sigma_{t0})}, \quad k = \frac{2}{\sqrt{3}}\frac{\sigma_{c0}\sigma_{t0}}{(\sigma_{c0} + \sigma_{t0})} \tag{2}$$

while h is a further material parameter, governing the possible hardening response beyond the initial yielding.

The plastic rate components $\dot{\varepsilon}^p_{ij}$ of the strain tensor are assumed to develop orthogonally to a potential surface $g(\sigma_{ij})$ as follows:

$$\dot{\varepsilon}^p_{ij} = \dot{\lambda}\frac{\partial g}{\partial \sigma_{ij}}, \quad g(\sigma_{ij}) = \sqrt{\frac{1}{2}\sigma'_{ij}\sigma'_{ij}} + \beta I_1 \tag{3}$$

where β represents the dilatancy coefficient.

Associative plasticity results as $\alpha = \beta$ while HHM model, typical of metals, is recovered as the internal friction angle α and the dilatancy coefficient β are set equal to zero. Notice that $\alpha = 0$ implies assuming equal yield limit in tension and compression, namely $\sigma_{c0} = \sigma_{t0}$, see relations (2), besides neglecting the volumetric contribution associated to I_1.

For the metal matrix composites under investigation, parameters α, β, k and h contained in the selected constitutive law represent effective material properties to be experimentally evaluated at the macroscopic scale together with the overall Young's modulus E and Poisson's ratio ν, which characterize the elastic response.

4. Mechanical characterization

The results reported in this Section concern the investigations performed on an Al/TiB_2 sample with 50% TiB_2 weight content and on an Al/ZrO_2 sample with 40% ZrO_2 weight content, in their preliminary production phase. The focus of the present research is in fact on modelling and parameter calibration issues rather than on the final material performances or on the production process. Details of these latter aspects can be found in the papers by Xie et al. (2003), Feng et al. (2005), and Gurt Santanach et al. (2009).

4.1. Indentation measurements

Instrumented indentation represents a practical methodology, extensively used for material characterization in industrial environments. Local and overall material and surface properties such as elastic modulus, yield strength, scratch resistance can be inferred from the curves representing imposed force versus penetration depth, derived from laboratory and in situ tests on various material

systems at different scale (Giannakopoulos and Suresh, 1997; Bhushan, 1999; Venkatesh et al., 2008; Dao et al. 2001; Capehart and Cheng, 2003; Bolzon et al., 2004, 2008; Bocciarelli and Bolzon, 2007; Bocciarelli et al., 2008).

The small available Al/TiB_2 and Al/ZrO_2 specimens (about 4 mm maximum dimension) were subjected to indentation under force control, up to 150 N load and then unloaded. Figs. 3 and 4 visualise the results of Rockwell test, where a rounded conical tip with 120° opening angle is pressed against the investigated materials. The maximum penetration depth is of the order of 100 μm, so that the response of the indented volumes can be considered representative of the mechanical macroscopic behaviour of the composites although some inhomogeneous distribution of micro-structural details, shown in Figs. 1 and 2, is reflected by the scatter of the indentation curves.

Experimental data have been averaged, and the corresponding mean values and variances used as input of the selected inverse analysis procedure, which combines the experimental results with the simulation of the test to return reliable estimates of the sought constitutive parameters.

The same material samples were subjected to pyramidal Vickers indentation as well, in two subsequent independent experimental campaigns. The so gathered information has been however used to verification purpose only, as reported in Section 5.

4.2. Inverse analysis

Quantitative calibration of parameters entering the selected constitutive model can be returned by inverse analysis procedures, which combine experimental data and the simulation of the laboratory test as shown, e.g., by Bui (1994), Stavroulakis et al. (2003), and Mroz and Stavroulakis (2004). The inverse analysis problem can be formulated

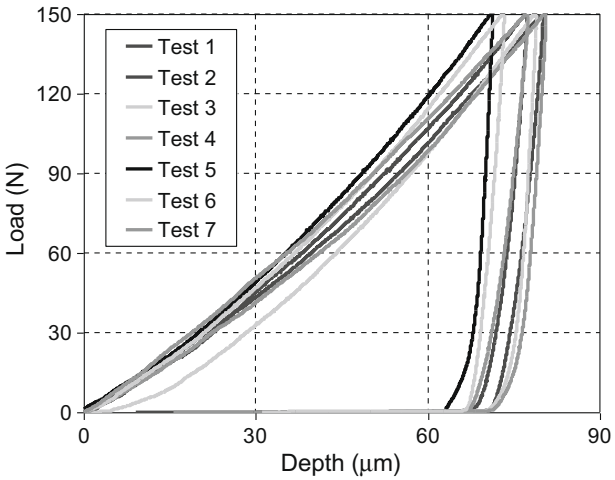

Fig. 3. Indentation curves obtained from conical (Rockwell) tests on Al/TiB_2 specimen.

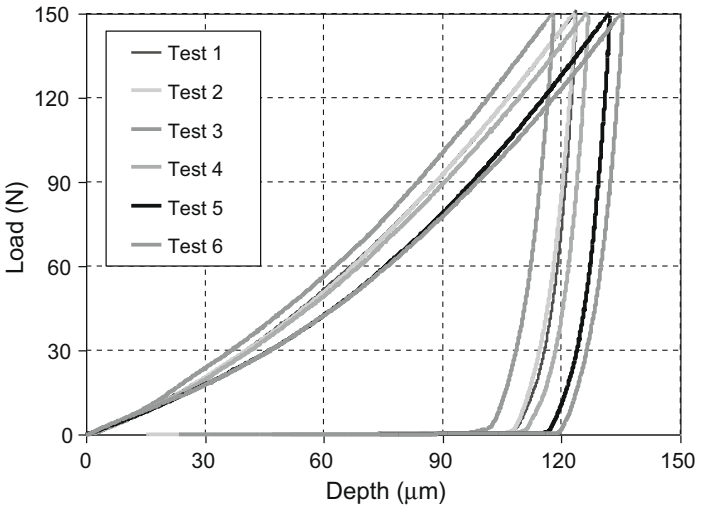

Fig. 4. Indentation curves obtained from conical (Rockwell) tests on Al/ZrO_2 specimen.

as the minimisation, with respect to the unknown parameters, of a norm that quantifies the overall discrepancy between the measured quantities and the corresponding values computed through a mathematical or numerical model.

In the present case, the indentation tests have been simulated in the large deformation regime by a finite element (FE) commercial code (Abaqus/Standard, 2006), as in previous analyses; see e.g. Dao et al. (2001), Capehart and Cheng (2003), Bolzon et al. (2004), and Bocciarelli and Bolzon (2007).

A detail of the discretized material region considered for the case of conical tip is shown in Fig. 5, account taken of the expected axis-symmetric overall response of the considered isotropic composites. Boundary conditions have been selected in view of the problem symmetry and of the assumption that outside the represented domain the material behaviour is linear elastic, to preliminarily perform condensation of the relevant degrees of freedom. The conical (Rockwell geometry) diamond tip has been modelled as perfectly rigid, while DP constitutive law with linear hardening rule describes the overall material response, see Section 3. Associative plasticity has been introduced as reasonable hypothesis in view of the metal content of the investigated samples, so that $\alpha = \beta$ in relations (2) and (3).

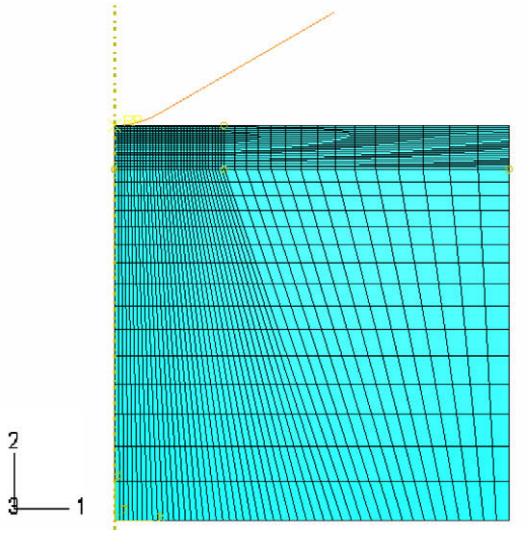

Fig. 5. Finite element model of Rockwell indentation test exploiting the expected axis-symmetry of the isotropic material response.

Poisson's ratio has been a priori fixed to the value 0.25, due to the expected low influence of this parameter on indentation results (Bolzon et al., 2004). The unknown overall material parameters to be returned by inverse analysis are, then: the elastic modulus *E;* the initial compression yield stress σ_{c0}; the internal friction angle α and the hardening modulus h. Let the relevant values be collected by vector $\mathbf{z}$.

Let the indentation forces F_i ($i = 1,\ldots,N$; here $N = 100$), selected in the range 0–150 N, sample the experimental mean indentation curves visualized in Figs. 6 and 7, and let d_{Mi} indicate the indentation depth corresponding to F_i. For any given value F_i, the FE test simulation returns the corresponding penetration depth $d_{Ci}(\mathbf{z})$, as a function of the input values given to the parameters contained in vector $\mathbf{z}$. Here subscripts C and M mean computed and measured, respectively.

The discrepancy between quantities returned by the experimental equipment and computed from the FE model can then be defined by the norm:

$$\omega(\mathbf{z}) = \sum_{i=1}^{N} \left(\frac{d_{Ci}(\mathbf{z}) - d_{Mi}}{w_i} \right)^2 \tag{4}$$

where w_i represent weights on the displacement components d_{Mi}, here assumed to coincide with the variances that quantify the measurement dispersion, also visualized in Figs. 6 and 7.

The optimum value of the sought parameters is represented by the entries of vector $\mathbf{z}_{opt}$, which corresponds to

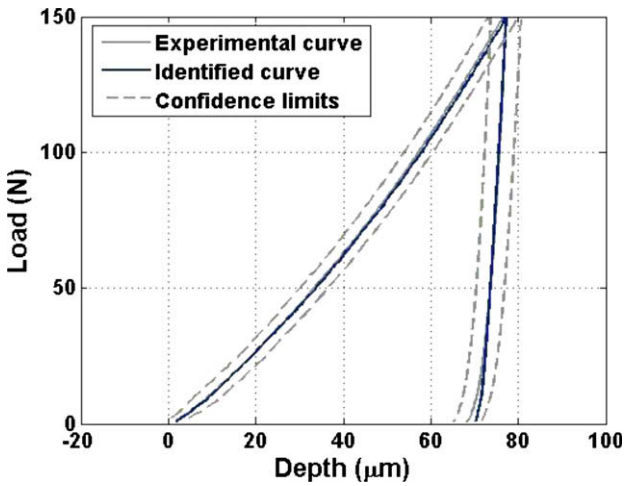

Fig. 6. Comparison between the experimental mean indentation curves obtained from conical (Rockwell) tests on the Al/TiB_2 specimen and the corresponding curves recalculated by the FE model, supplemented by the identified material parameter set.

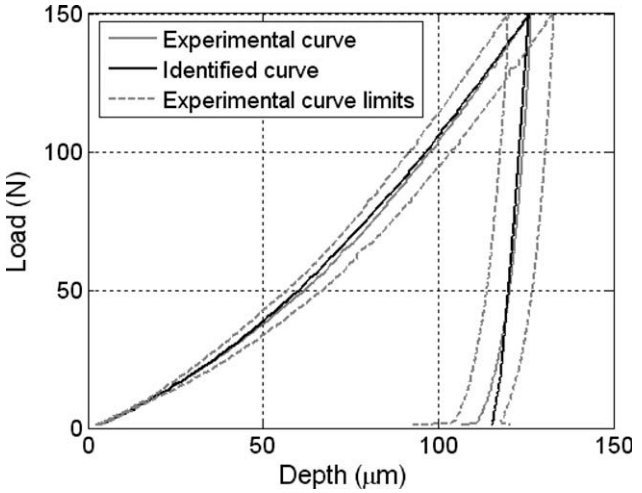

Fig. 7. Comparison between the experimental mean indentation curves obtained from conical (Rockwell) tests on the Al/ZrO_2 specimen and the corresponding curves recalculated by the FE model, supplemented by the identified material parameter set.

Table 1
Identified material properties after different initializations of the discrepancy minimisation algorithm.

	Elastic modulus E (GPa)	Initial yield limit in compression σ_{c0} (MPa)	Internal friction angle α (°)	Hardening modulus h (MPa)
Al/TiB_2	57.9 (±3.7)	240.4 (±36.5)	10.7 (±4.3)	1032 (±91)
Al/ZrO_2	28.0 (±1.0)	74.3 (±12.6)	14.8 (±4.1)	838 (±102)

the minimum discrepancy. These values can be returned by a number of numerical methods implemented in widely available optimization tools (e.g. Matlab, 2004). For the present application, the so-called Trust Region algorithm (Coleman and Li, 1996) has been satisfactorily employed. Details can be found in the reference manuals (Matlab, 2004).

In the present context, the discrepancy function $\omega(\mathbf{z})$ is expected to be non-convex and to admit multiple minimum points, often practically equivalent from the engineering point of view, in the sense that the corresponding parameter values approximate to the same extent the available experimental data and return comparable representation of the real material behaviour, consistently with the selected constitutive model. The optimization algorithm is hence run several times, starting from different initial parameter sets. Results are given in Table 1 in terms of the average and of the standard deviation of the converged values, which returned small similar values of $\omega(\mathbf{z}_{opt})$. The dispersion on most identified material parameter values is well below the scatter of the collected experimental data. The biggest uncertainty is observed for the internal friction angle, which however assumes values far from zero in any case.

The accuracy of the selected material model and of the optimal parameter set obtained from the present identification procedure can be appreciated by the comparison of the initial experimental information and of the corresponding recalculated curves, also drawn in Figs. 6 and 7.

5. Validation

The capability of the selected constitutive model, supplemented by the identified parameter values, to represent the real material behaviour has been further verified making use of experimental information collected from Vickers pyramidal indentation of the same material specimens, performed in two subsequent experimental campaigns. These data, represented in Figs. 8–11, were not considered in the former parameter identification phase.

It is worth noticing that the curves obtained from Vickers tests are more scattered than in the case of Rockwell indentation, especially for the second set of experiments. One reason for this dispersion is the sharp pyramidal tip which can promote the growth of existing material defects and the consequent morphological changes at the microstructural level.

For Vickers indentation setup, the experimental apparatus automatically returns the so-called reduced modulus E_r, evaluated according to the popular formula by Oliver and Pharr (1992, 2004):

$$E_r = c\frac{S}{\sqrt{A}} \tag{5}$$

where the contact stiffness S represents the initial slope of the unloading curve, c is a calibration parameter that depends on the indenter geometry and A is the estimated contact area at the applied maximum load.

The average value and the variance of the reduced modulus E_r returned by the available equipment (Zwick/Roell ZHU 0,2) are listed in Table 2 for both material specimens, separately for each experimental campaign.

The reduced modulus E_r is correlated to initial elastic modulus E of the tested material by the expression:

$$\frac{1}{E_r} = \frac{1-\nu^2}{E} + \frac{1-\nu_i^2}{E_i} \tag{6}$$

where E_i and ν_i represent the elastic moduli of the diamond indenter tip (here assumed to be equal to 1140 GPa and

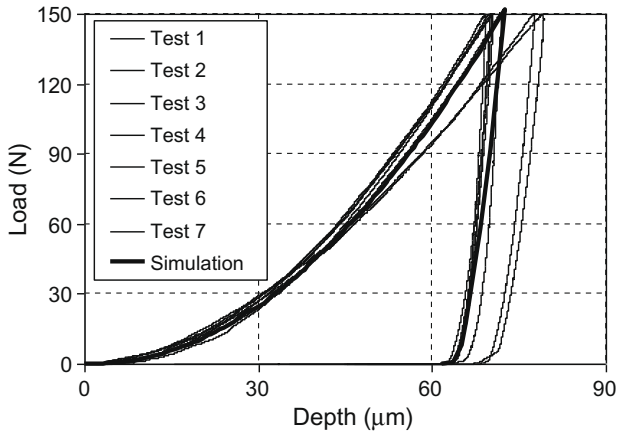

Fig. 8. Comparison between the experimental curves obtained from the first pyramidal (Vickers) indentation campaign, sampling different locations of the same Al/TiB_2 specimen, and the corresponding FE simulation based on parameter values identified from Rockwell indentation data.

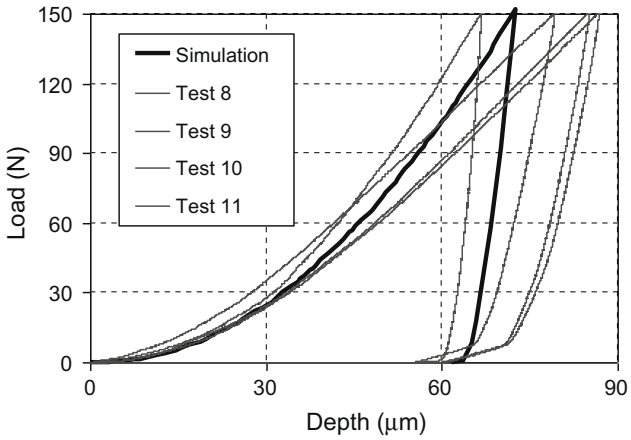

Fig. 9. Comparison between the experimental curves obtained from the second pyramidal (Vickers) indentation campaign, sampling different locations of the same Al/TiB_2 specimen, and the corresponding FE simulation based on parameter values identified from Rockwell indentation data.

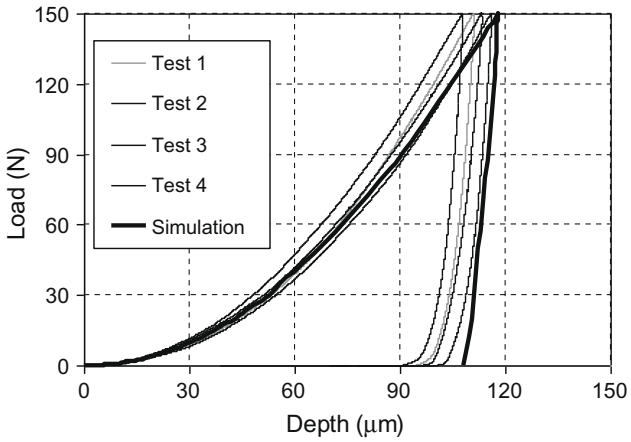

Fig. 10. Comparison between the experimental curves obtained from the first pyramidal (Vickers) indentation campaign, sampling different locations of the same Al/ZrO_2 specimen, and the corresponding FE simulation based on parameter values identified from Rockwell indentation data.

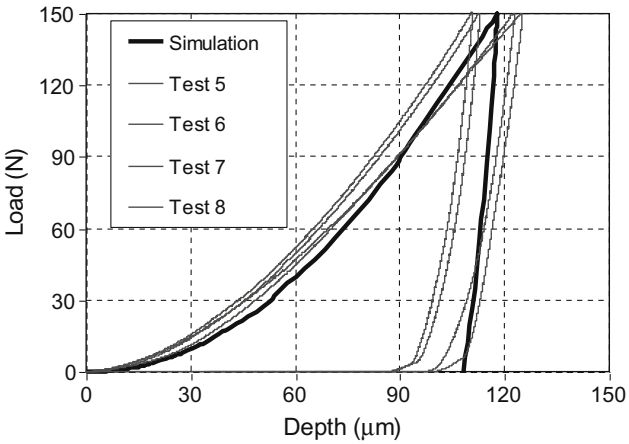

Fig. 11. Comparison between the experimental curves obtained from the second pyramidal (Vickers) indentation campaign, sampling different locations of the same Al/ZrO_2 specimen, and the corresponding FE simulation based on parameter values identified from Rockwell indentation data.

Table 2
Reduced modulus E_r returned by the indentation equipment and the corresponding initial elastic modulus E in the two subsequent experimental campaigns; see Figs. 8–11.

	1st Experimental campaign		2nd Experimental campaign	
	E_r (GPa)	E (GPa)	E_r (GPa)	E (GPa)
Al/TiB_2	101.8 ± 29.3	104.7 ± 28.2	32.7 ± 1.3	31.6 ± 1.2
Al/ZrO_2	37.5 ± 4.8	36.3 ± 4.5	20.8 ± 3.9	19.9 ± 3.7

0.07, respectively, as in most literature), while ν represents the Poisson ratio of the indented material (here assumed equal to 0.25, as above).

The resulting average E values and the corresponding variances are also listed in Table 2 for both material specimens. Fair agreement is found with the identification results listed in Table 1 for the Al/ZrO_2 compound, having the quite homogeneous microstructure shown in Fig. 2, while much bigger differences can be noticed for Al/TiB_2 elastic modulus. In this latter case, however, the experimental scatter is also rather high, especially for the values concerning the first experimental campaign, which was performed concurrently with the Rockwell indentation tests. It is however worth to be remembered that Oliver and Pharr (1992, 2004) approach is semi-empirical, based on some data fitting concerning metals and, therefore, is to be considered fully reliable for this material class only; see also Bolzon et al. (2004).

A strong reduction of the elastic modulus (likely associated to similar deterioration of the remaining mechanical properties) was observed in both material systems as the investigation was repeated and the number of tests increased. In fact, due to the small dimensions of the available specimens (about $2 \times 4\,mm^2$ free surface), it becomes more and more difficult to find material portions completely unaffected by previous indentations.

Vickers test has been simulated by the 3D FE model visualized in Fig. 12. Also in this case, the assumed isotropic overall material response and the symmetries of the pyramidal tip allowed to reduce the modelled material volume with some computing savings, though much smaller than in the previous axis-symmetric case.

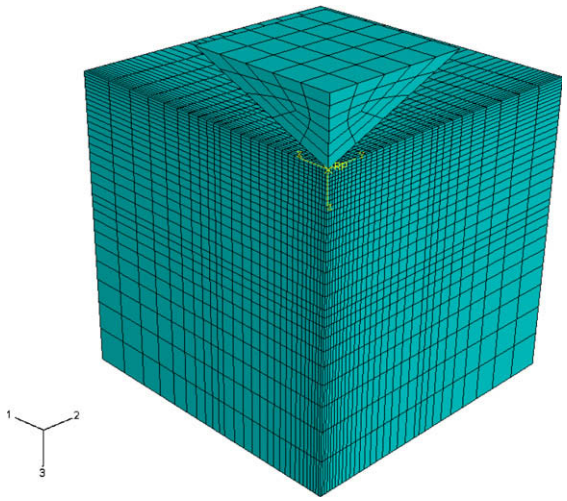

Fig. 12. Finite element model of Vickers indentation test exploiting the symmetries of the pyramidal tip.

The material parameters obtained from the previous identification step, listed in Table 1, return the computed indentation curves shown in Figs. 8–11 together with the experimental results. A good matching is observed on average for both metal-ceramic compounds, especially with those relevant to the first Vickers test series (Figs. 8 and 10).

6. Theoretical bounds on material properties

Homogenization theories have been developed for composites with the attempt of replacing experimentally-based material characterization procedures, to be performed at the macroscopic scale, by some correlation formula based on average microscopic quantities weighted by the spatial distribution of volumetric ratios; see e.g. Sanchez-Palencia, 1980.

Lower and upper bounds to the overall values of the elastic moduli can be given by assuming that either the stress (Reuss model) or the strain (Voigt model) distribution remains uniform in uniformly loaded material sample, thus leading to the estimates:

$$E_R = \frac{E_c E_m}{V_c E_m + V_m E_c}, \quad E_V = V_c E_c + V_m E_m \tag{7}$$

where V_c and V_m (=$1 - V_c$), E_c and E_m represent volume fraction and Young's modulus of the ceramic and of the metal phase, respectively, in the present application.

These simple classical bounds can be rather loose and, in some situations, better fit with available experimental data can be obtained by some modification of the above classical rules; see, e.g. Tamura et al. (1973), Moon et al. (2005), and Bocciarelli et al. (2008).

Bounds (7) and their main modifications are however based on the (strong) assumption that the composite behaves as a two-phase continuum medium, with perfect continuity across the interfaces between the different components, neglecting any possible influence of micro-voids, damages or defects on the effective material properties.

Ensuring good bonding between dissimilar metallic and non-metallic particles is one of the main issues in the production processes of sintered metal matrix composites, but this goal is not easily and not always achieved, with strong effects on the overall mechanical performances; see e.g. El-Hadek and Kaytbay (2009) and references therein.

Damage evolution under loading of metal matrix composites with interpenetrating network structure was also reported, e.g. by Bruck and Rabin (1999). Consistently with their observations, Bruck and Rabin (1999) suggested that a lower bound to the elastic modulus of these material systems, more realistic than E_R (7), could be derived by considering any detached or damaged material portion to behave as an equivalent porous inclusion in the remaining interconnected material system. An empirical formula developed by Coble and Kingery (1956) for porous ceramics was shown to satisfactorily correlate the overall elastic modulus of the damaged composite to the so evaluated amount of equivalent porosity and to the elastic modulus of the completely dense matrix as

$$E_{CK} = E_m(1 - 1.9V_c + 0.9V_c^2) \tag{8}$$

or

$$E_{CK} = E_c(1 - 1.9V_m + 0.9V_m^2) \tag{9}$$

depending on whether the connective function is accomplished by the metal or by the ceramic phase in the damaging material system under investigation.

Table 3
Reuss (E_R), Voigt (E_V) and Coble–Kingerin (E_{CK}) bounds on elastic moduli, relations (7)–(9).

	V_c	V_m	E_R (GPa)	E_V (GPa)	E_{CK} (GPa)
Al/TiB_2	38.5	61.5	104.6	235.4	28.2
Al/ZrO_2	23.4	76.6	82.5	100.4	14.5

The results of these theoretical bounds are compared in Table 3 for the considered ZrO_2 and TiB_2 composites.

7. Discussion

The purpose of the present research work was to verify whether: (i) Drucker–Prager (DP) model, sensitive to hydrostatic stress components, is more suitable than Hencky–Huber–Mises (HHM) yield criterion, based on J_2 flow theory, to describe the mechanical response of the aluminium-based metal matrix composites under consideration; (ii) classical or modified mixture rules can be used to estimate the values of the parameters entering these models and representing overall material properties.

HHM criterion can be recovered from DP model as the value of the internal friction angle α is set equal to zero. In the present work, this parameter has been inferred from the available experimental information gathered from conical Rockwell indentation of the two metal matrix composite samples, see the results listed in Table 1. The scatter on the value of the internal friction angle returned by the exploited inverse analysis procedure is relatively large, nevertheless α values were found much larger than zero in all considered situations, thus indicating that hydrostatic stress components play some significant role in controlling the mechanical response of these materials.

The appropriateness of DP material model has been further verified against the results of pyramidal Vickers indentation, also performed in the available material specimens. A good matching between experimental results and numerical predictions has been observed, on average, despite the fact that the sharp corners of the pyramidal tip can easily induce the formation and the propagation of micro-cracks, which change the microscopic material morphology and lead to the deterioration of the overall material properties, e.g. quantified by the reduction of the effective elastic modulus listed in Table 2. These features are reflected by the increased scatter of the experimental results and by the progressively reduced material stiffness and strength, reflected by the increasing penetration depths for the same applied load level as the tests performed on the same small specimen are repeated and the usually negligible far-field effect of previous indentation is enhanced.

According to classical homogenization theory, the overall elastic modulus of a two-phase composite roughly falls within the range defined by Reuss and Voigt estimates, E_R and E_V, respectively, relations (7). Table 3 reports these bounds, evaluated for typical literature values of the Young modulus of Al, ZrO_2 and TiB_2 (70, 200 and 500 GPa, respectively), adopting material densities 2700, 5900 and 4320 kg/m^3, respectively, to transform the considered

weight content (see Section 2) into the corresponding volume fractions. Notice that the Young modulus estimates inferred from the performed indentation experiments, either by inverse analysis (see Table 1) or by the classical Oliver and Pharr formulae, relations (5) and (6) (values listed in Table 2), are systematically smaller (even much smaller) than the rough lower bound E_R. This result evidences the strong influence, on the overall mechanical properties, of the material defectiveness resulting from the production process and enhanced by local damaging produced during material testing.

According to Bruck and Rabin (1999), the empirical formulae (8) and (9), inferred from that developed by Coble and Kingery (1956) for porous ceramics, correlate in a satisfactory manner the overall elastic modulus of the damaged composite to the elastic modulus of the completely dense matrix, account taken of the amount of equivalent porosity defined by the lack of continuity in the material microstructure.

In the present context, the composite matrix is assumed to coincide with the metal phase and the equivalent porosity is identified with the ceramic volume fraction V_c in the case of the Al/TiB_2 composite, where ceramic particles are poorly interconnected, see Fig. 2. The lower bound estimate of the corresponding elastic modulus is then given by relation (8). Fig. 3 shows, instead, a rather continuous ZrO_2 extension with some embedded Al zones. In this case, the most appropriate lower bound estimate is therefore defined by relation (9). These values are listed in Table 3 for both considered material systems. Notice that these values are rather close to the average elastic moduli obtained from the experimental information gathered in the second campaign, which clearly induced some extensive damaging in the material, evidenced by the shift toward increasing penetration depth of the indentation curves drawn in Figs. 9 and 11. Notice also that this drift is more pronounced in the case of Al/TiB_2 composite (3 out of 4 curves of this second set shift on the right of the computed reference one), where elastic moduli listed in Table 2 are closer to their corresponding lower bounds, Table 3.

8. Closing remarks

The present research was intended to verify whether the classical Hencky–Huber–Mises (HHM) plasticity model or the more general Drucker–Prager (DP) one, which includes HHM as a special case but more accurately describes the main features of the mechanical response of most ceramics, were better suited to describe the overall mechanical response of aluminium-based composites produced by spark plasma sintering (SPS). The results of the performed experimental-numerical study show that the material response is better represented when hydrostatic stress components are taken into account by the constitutive model also beyond the elastic range, as in DP formulation.

It was further shown that embedded defects and local damages play an essential role in defining the overall material properties, as earlier observed for different material systems by Bruck and Rabin (1999). Classical mixture laws obtained from homogenization rules that neglect micro-structural details, fail in returning reliable quantitative prediction of constitutive parameters of the investigated metal matrix composites even in the elastic range.

Acknowledgement

The results presented in this paper have been obtained in a research work partially funded by the European Commission through the FP6 Network of excellence of Knowledge-based Multicomponent Materials for durable and safe performance, KMM-NoE, Project No. NMP3-CT-2004-502243.

References

Bhattacharyya, M., Kapuria, S., Kumar, A.N., 2007. On the stress to strain transfer ratio and elastic deflection behavior for Al/SiC functionally graded material. Mech. Adv. Mater. Struct. 14, 295–302.

Bhushan, B., 1999. Handbook of Micro/Nano Tribology. CRC Press, Boca Raton, FL.

Bocciarelli, M., Bolzon, G., 2007. Indentation and imprint mapping for the identification of constitutive parameters of thin layers on substrate: perfectly bonded interfaces. Mater. Sci. Eng. A 448, 303–314.

Bocciarelli, M., Bolzon, G., Maier, G., 2008. A constitutive model of metal–ceramic functionally graded material behavior: formulation and parameter identification. Comput. Mater. Sci. 43, 16–26.

Bolzon, G., Bocciarelli, M., Chiarullo, E.J., 2008. Mechanical characterization of materials by micro-indentation and AFM scanning. In: Bhushan, B., Fuchs, H. (Eds.), Applied Scanning Probe Methods XII Characterization. Springer-Verlag, Heidelberg, pp. 85–120.

Bolzon, G., Maier, G., Panico, M., 2004. Material model calibration by indentation, imprint mapping and inverse analysis. Int. J. Solid Struct. 41, 2957–2975.

Bruck, H.A., Rabin, R.H., 1999. Evaluating microstructural and damage effects in rule-of-mixtures predictions of the mechanical properties of Ni–Al_2O_3 composites. J. Mater. Sci. 34, 2241–2251.

Bui, H.D., 1994. Inverse Problems in the Mechanics of Materials: An Introduction. CRC Press, Boca Raton, FL.

Capehart, T.W., Cheng, Y.-T., 2003. Determining constitutive models from conical indentation: sensitivity analysis. J. Mater. Res. 18, 827–832.

Coble, L., Kingery, W.D., 1956. Effect of porosity on physical properties of sintered alumina. J. Am. Ceram. Soc. 39, 377–385.

Coleman, T.F., Li, Y., 1996. An interior trust region approach for nonlinear minimisation subject to bounds. SIAM J. Optim. 6, 418–445.

Dao, N., Chollacoop, N., van Vliet, K.J., Venkatesh, T.A., Suresh, S., 2001. Computational modeling of the forward and reverse problem in instrumented indentation. Acta Mater. 49, 3899–3918.

El-Hadek, M.A., Kaytbay, S., 2009. Al_2O_3 particle size effect on reinforced copper alloys: an experimental study. Strain 45, 506–515.

Feng, H., Jia, D., Zhou, Y., 2005. Spark plasma sintering reaction synthesized TiB reinforced titanium matrix composites. Composites A 36, 558–563.

Giannakopoulos, A.E., Suresh, S., 1997. Indentation of solids with gradients in elastic properties: Part ii. Axisymmetric indentors. Int. J. Solids Structures 34, 2393–2428.

Giannakopoulos, A.E., 2002. Indentation of plastically graded substrates by sharp indentors. Int. J. Solid Struct. 39, 2495–2515.

Gu, Y., Nakamura, T., Prchlik, L., Sampath, S., Wallace, J., 2003. Microindentation and inverse analysis to characterize elastic–plastic graded materials. Mat. Sci. Eng. A 345, 223–233.

Gurt Santanach, J., Estournès, C., Weibel, A., Peigney, A., Chevallier, G., Laurent, Ch., 2009. Spark plasma sintering as a reactive sintering tool for the preparation of surface-tailored Fe–$FeAl_2O_4$–Al_2O_3 nanocomposites. Scripta Mater. 60, 195–198.

HKS Inc., 2006. ABAQUS/Standard, Theory and User's Manuals, release 6.6-1. Pawtucket, RI, USA.

Hulbert, D.M., Jiang, D., Dudina, D.V., Mukherjee, A.K., 2009. The synthesis and consolidation of hard materials by spark plasma sintering. Int. J. Refract. Met. Hard Mater. 27, 367–375.

Ichikawa, K., 2001. Functionally Graded Materials in the 21st Century. A Workshop on Trends and Forecasts. Springer, Berlin.

Jin, Z.H., Paulino, G.H., Dodds Jr., R.H., 2003. Cohesive zone fracture modeling of elastic–plastic crack growth in functionally graded materials. Eng. Fract. Mech. 70, 1885–1912.
Moon, R.J., Tilbrook, M., Hoffman, M., Neubrand, A., 2005. Al–Al_2O_3 composites with interpenetrating network structures: composite modulus estimation. J. Am. Ceram. Soc. 88, 666–674.
Mroz, Z., Stavroulakis, G. (Eds.), 2004. Parameter Identification of Materials and Structures. Springer-Verlag, Berlin.
Nakamura, T., Wang, T., Sampath, S., 2000. Determination of properties of graded materials by inverse analysis and instrumented indentation. Acta Mater. 48, 4293–4306.
Oliver, W.C., Pharr, G.M., 1992. An improved technique for determining hardness and elastic modulus using load and displacement sensing indentation experiments. J. Mater. Res. 7, 1564–1583.
Oliver, W.C., Pharr, G.M., 2004. Measurement of hardness and elastic modulus by instrumented indentation: advances in understanding and refinements to methodology. J. Mater. Res. 19, 3–20.
Omori, M., 2000. Sintering, consolidation, reaction and crystal growth by the spark plasma system (SPS). Mater. Sci. Eng. A287, 183–188.
Sanchez-Palencia, E., 1980. Non-homogeneous media and vibration theory. Lecture Notes in Physics, vol. 127. Springer-Verlag, Berlin.
Stavroulakis, G., Bolzon, G., Waszczyszyn, Z., Ziemianski, L., 2003. Inverse analysis. In: Karihaloo, B., Ritchie, R.O., Milne, I. (Eds.), Comprehensive Structural Integrity, vol. 3. In: de Borst, R., Mang, H.A. (Eds.), Numerical and Computational Methods. Elsevier Science Ltd., Kidlington, UK, pp. 685–718 (Chapter 13).
Tamura, I., Tomota, Y., Ozawa, H., 1973. Strength and ductility of Fe–Ni–C alloys composed of austenite and martensite with various strength. In: Proceeding of the Third International Conference on Strength of Metals and Alloys, vol. 1. Institute of Metals, Cambridge, pp. 611–615.
The Math Works Inc, 2004. Matlab User's Guide and Optimization Toolbox, release 6.13. Natick, MA, USA.
Venkatesh, T.A., van Vliet, K.J., Giannakopoulos, A.E., Suresh, S., 2000. Determination of elasto-plastic properties by instrumented sharp indentation: guidelines for property extraction. Scripta Mater. 42, 833–839.
Xie, G., Ohashi, O., Chiba, K., Yamaguchi, N., Song, M., Furuya, K., Noda, T., 2003. Frequency effect on pulse electric current sintering process of pure aluminium powder. Mater. Sci. Eng. A359, 384–390.